Chinese Chemical Letters 35 (2024) 108577

Contents lists available at ScienceDirect

Chinese Chemical Letters

journal homepage: www.elsevier.com/locate/cclet

mtDNA-triggered pH response signal-amplified fluorescent probe for multiple cell discrimination

Tianping Xia[a], Yanxian Hou[a], Zhuoran Xia[a], Gengwen Chen[b], Peichen Tang[a], Jiangli Fan[a,c,*], Xiaojun Peng[a,c]

[a] State Key Laboratory of Fine Chemicals, Frontiers Science Center for Smart Materials Oriented Chemical Engineering, Dalian University of Technology, Dalian 116024, China
[b] Hematology Reagent R&D Department, Mindray Bio-medical Electronics Co. Ltd., Shenzhen 518132, China
[c] Research Institute of Dalian University of Technology in Shenzhen, Shenzhen 518057, China

ARTICLE INFO

Article history:
Received 3 April 2023
Revised 8 May 2023
Accepted 14 May 2023
Available online 19 May 2023

Keywords:
Fluorescence probe
Mitochondrial DNA
pH response
Peripheral blood cells
Multiple cell detection

ABSTRACT

Developing fluorescence probes with multiple responses has vital significance but remains challenging. Herein, for the first time, we present a mitochondrial DNA (mtDNA)-triggered pH response signal-amplified fluorescent probe (QCY-DBT) for multiple cell detection. The probe exhibited a large stokes shift (229 nm), excellent DNA selectivity over RNA, and ultrasensitivity of detection limit (DL; 74.0 ng/mL). Thus, QCY-DBT was successfully applied to analyze multiple human peripheral blood cells and visualize mtDNA in healthy and apoptotic cells. In the tumor acidic environment (pH 6.0–7.0), the absorbance of QCY-DBT at 436 nm increased, and the fluorescence signal (665 nm) was amplified by mtDNA, which enabled the direct observation of tumor cells. Our study provides help in designing smart probes with multiple responses for efficient abnormal cell detection.

Human peripheral blood cells mainly contain white blood cells (WBCs), red blood cells (RBCs), and platelets (PLTs) [1,2]. Abnormal changes in the count of these blood cells are mainly related to pathology, such as acute or chronic leukemia [3], iron-deficiency anemia [4], and hemolytic anemia [5]. The content of nucleic acids differs in different blood cells. For example, the DNA content, including mitochondrial DNA (mtDNA) and nuclear DNA, of WBCs were ranked as follows, from highest to lowest: monocytes > lymphocytes > neutrophils > eosinophils > basophils [6]. Notably, due to the lack of intron and histone protection, imperfection of the repair function, and high susceptibility to damage, mtDNA exhibits a 10-fold higher incidence of damage than nuclear DNA [7–10]. However, mtDNA plays unique roles in bioactive processes, including oxidative phosphorylation, the generation of ATPase, nicotinamide adenine dinucleotide (NADH) dehydrogenase, and cytochrome oxidase [11,12], which is related to the development of cancer cells, including their proliferation and apoptosis [13–15]. Furthermore, the extracellular pH of normal tissue and blood is maintained at 7.4, whereas extracellular acid fluid (pH 6.0–7.0) is a hallmark of solid tumors due to a lack of full glucose oxidation capacity of proliferating tumor cells to produce energy [16–19]. It is crucial to develop mtDNA-specific and pH response technologies that can simultaneously track mtDNA and pH changes in real time, especially for identifying blood cells, cancer cells, and their apoptosis.

Fluorescent probes have emerged as indispensable chemical tools to detect nucleic acids, pH, and other biological substances in living cells [20–27]. However, most DNA probes concentrated on nuclear DNA [28–31], and currently, some available mtDNA probes are limited by insufficient sensitivity, specificity, or small stokes shifts with low signal-to-noise ratios [32]. Furthermore, since pH changes between cancerous and normal tissues are minimal [33–35]. The efficacy of the pH fluorescent probes remains challenging, although a limited number of examples have been reported [36–38]. Fluorescence probes with multiple responses are more efficient in meeting the detection demand in complex physiological environments than single response fluorescence probes [39,40]. Until now, no probe has been reported for both mtDNA and pH.

Herein, we report an mtDNA-specific and pH response near-infrared (NIR) fluorescence probe (QCY-DBT) based on heptamethine cyanine dyes (Fig. 1a). QCY-DBT displays a large stokes shift, ultrasensitivity to DNA, and excellent DNA selectivity over RNA. Thus, QCY-DBT was successfully combined with a commercial probe of reticulocytes for multiple blood cell detection in flow cytometry, including four kinds of leukocytes, reticulocytes, and platelets. Furthermore, the specific mitochondria anchoring was

* Corresponding author.
E-mail address: fanjl@dlut.edu.cn (J. Fan).

https://doi.org/10.1016/j.cclet.2023.108577
1001-8417/

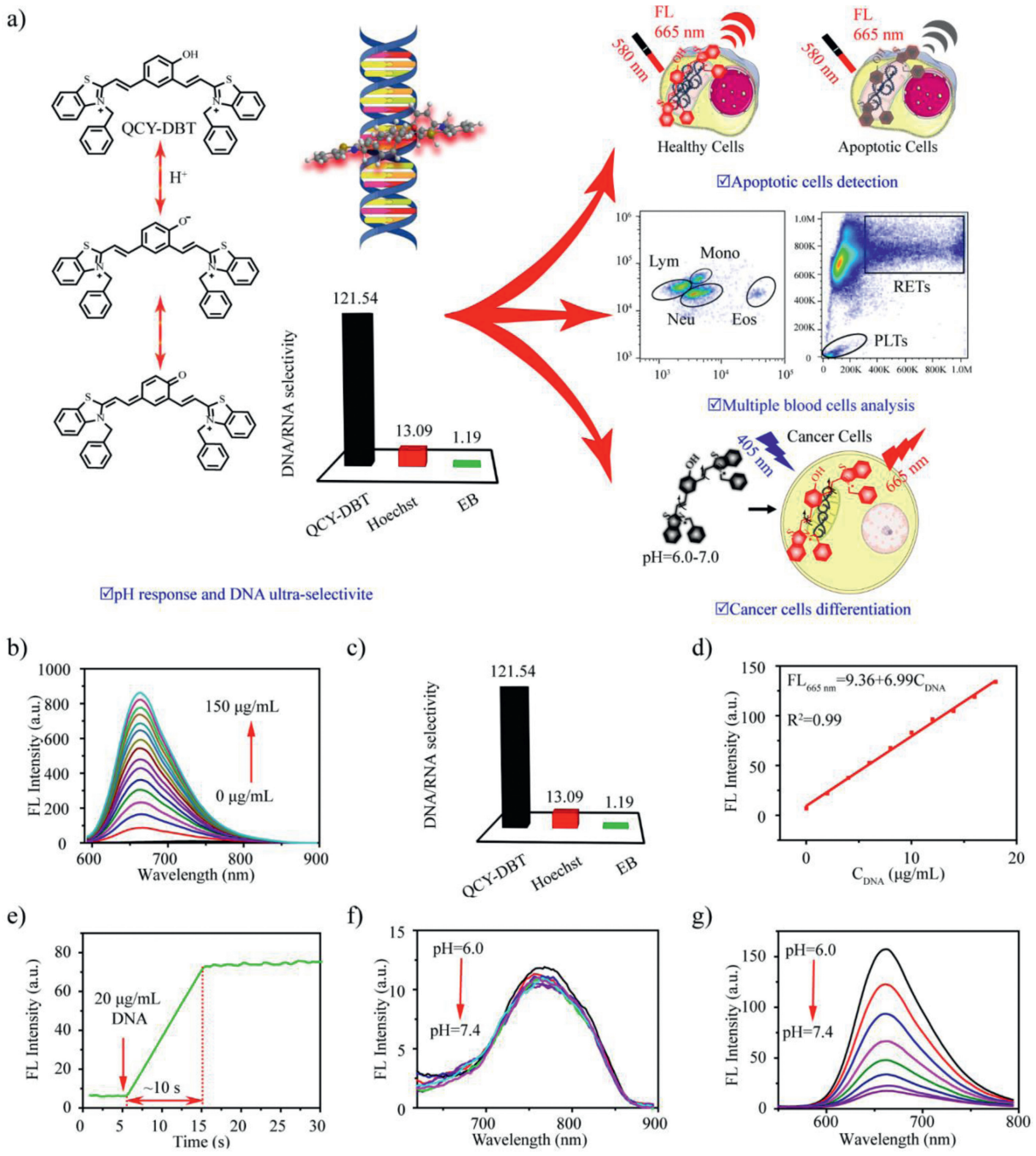

Fig. 1. (a) Molecular structure of QCY-DBT and its applications for multiple cell detection. (b) Fluorescence emission spectra during the titration of a solution of QCY-DBT (8 μmol/L) with CT DNA (0–150 μg/mL) (λ_{ex} = 580 nm). (c) Comparison of DNA/RNA selectivity of QCY-DBT, Hoechst 33342, and EB. (d) Linear response of QCY-DBT for DNA in the emission spectrum, $FL_{665nm}=9.36+6.99C_{DNA}$ ($R^2=0.99$). (e) Time course of fluorescence intensity of QCY-DBT (8 μmol/L) at 665 nm after addition of CT DNA; time range = 0–30 s. (f) Fluorescence emission spectra of QCY-DBT (8 μmol/L) in PBS buffer solution at various pH (6.0–7.4) (λ_{ex} = 436 nm). (g) Fluorescence emission spectra of QCY-DBT (8 μmol/L) with a fixed concentration of DNA (10 μg/mL) in PBS buffer solution at various pH (6.0–7.4) (λ_{ex} = 436 nm).

also observed, thus realizing the specific recognition of mtDNA in living cells. By monitoring the changes in mtDNA, apoptotic cells were distinguished. In the acid environment of tumors, the absorbance of QCY-DBT at 436 nm increased, and the fluorescence signal (665 nm) was amplified by mtDNA in living cells. As a result, cancer cells were recognized with much higher fluorescence intensity than normal cells. As far as we know, this is the first demonstration of an mtDNA-triggered pH response signal-amplified fluorescent probe for detecting apoptotic cells, cancer cells, and multiple blood cells.

N-Benzyl-2-methylbenzothiazolium bromide salt was demonstrated to prefer accumulating in mitochondria in our previous study [41]. Phenol has been reported as a pH-sensitive group [42,43]. Therefore, two *N*-benzyl-2-methylbenzothiazolium bromide salts were connected with phenol by a condensation reaction and finally synthesized a one donor/two acceptors probe named QCY-DBT according to the routes in Scheme S1 (Supporting information). The V-shaped structure could make QCY-DBT selectively bind to the minor grooves of DNA. The chemical structures of QCY-DBT and all synthetic intermediates were fully confirmed by ^{1}H

nuclear magnetic resonance (NMR), ^{13}C NMR, and electrospray ionization mass spectrometry (ESI-MS) analytical data (Figs. S24–S26 in Supporting information).

The absorption and emission spectra of QCY-DBT (8.0 μmol/L) in the absence and presence of calf thymus DNA (CT DNA) in PBS (10.0 mmol/L, pH 7.4) were recorded and are presented in Fig. S1 (Supporting information). Free QCY-DBT (8.0 μmol/L) exhibited two strong absorption peaks at 503 nm and 580 nm (Fig. S1a) and emitted a weak near-infrared fluorescence signal at 730 nm (Fig. S1b). The absorption band at 580 nm originated from the delocalization of π-electrons between phenolic oxygen and *p*-substituted benzothiazolium vinyl moiety in QCY-DBT, while the band at 503 nm is from the similar conjugation of *o*-substituted benzothiazolium vinyl moiety in QCY-DBT. The fluorescence emission of QCY-DBT was blue and shifted to 665 nm, and the fluorescence intensity ($F^{CT\ DNA}/F^{free}$) of QCY-DBT increased 122-fold upon binding to CT DNA (Fig. 1b and Fig. S2 in Supporting information), while almost no fluorescence increase was observed upon binding to RNA ($F^{RNA}/F^{free} = 0.8$) (Fig. S3 in Supporting information). The value of DNA/RNA specificity ($F^{CT\ DNA}/F^{RNA}$) of QCY-DBT (121.54) was higher (9.3-fold) than both Hoechst 33342 (13.09) and ethidium bromide (EB) (1.19) (Fig. 1c and Fig. S4 in Supporting information). Furthermore, the fluorescence intensity of QCY-DBT at 665 nm exhibited a good linear relationship with increasing concentrations of CT DNA over a range of 0–18 μg/mL ($FL_{665\ nm} = 9.36 + 6.99C_{DNA}$, $R^2 = 0.99$), and the minimum detection limit of QCY-DBT for DNA was 74.0 ng/mL (Fig. 1d and Fig. S5 in Supporting information). Fluorescence titration with two oligonucleotides $ds(A\text{-}T)_{20}$ and $ds(G\text{-}C)_{20}$ revealed that QCY-DBT binds preferentially to $ds(A\text{-}T)_{20}$ (Table S1 and Fig. S6 in Supporting information), suggesting that QCY-DBT specifically binds to the AT base-pair of nucleic acids. Indeed, amino acids (L-Val, D-Asp, L-His), glucose, glutathione (GSH), protein (bovine serum albumin), and yeast RNA did not result in an obvious interaction at 4-fold excess concentrations (Fig. S7 in Supporting information). QCY-DBT responded to viscosity and polarity weakly (Fig. S8 in Supporting information), and it did not affect the detection of DNA. Time-dependent (0–30 s) fluorescence responses (665 nm) of QCY-DBT in the presence of CT DNA indicated that the binding process could be completed within 10 s (Fig. 1e). In Fig. S9a (Supporting information), with the change in pH from 2 to 8, the absorbance of QCY-DBT at 436 nm decreased, and the absorbance at 580 nm increased gradually. When excited at 580 nm, the fluorescence intensity increased with the pH (Fig. S9b in Supporting information). Due to the effect of twisted intramolecular charge transfer, the fluorescence signal of QCY-DBT only varied a little with the pH ($F^{pH=6.0}/F^{pH=7.4} = 1.1$) (Fig. 1f). However, with a fixed concentration of CT DNA (20 μg/mL), the fluorescence intensity of QCY-DBT significantly decreased upon excitation at 436 nm (Fig. 1g). When CT DNA was added, the fluorescence signal at pH 6.0 was ~8.95-fold higher than the pH at 7.4, which was ~7.85-fold higher than the solution without CT DNA. Therefore, the pH response signal of QCY-DBT was amplified by DNA, making pH detection possible. The above spectral results indicated that QCY-DBT was able to monitor the changes in DNA and pH in complicated biological environments.

To determine the binding mode of QCY-DBT to CT DNA, thermal melting (T_m) analysis was first conducted under ambient conditions. The intercalative binding mode of small molecules with the double-helical DNA raises the T_m by 5–8 °C, while non-intercalative binding, such as electrostatic or groove binding, causes less or no change in T_m [44]. As presented in Fig. S10a (Supporting information), the T_m of CT DNA was not affected by dimethyl sulfoxide (DMSO) and only increased a little (2.0 °C) with the addition of QCY-DBT (8 μmol/L), illustrating that the binding mode of QCY-DBT with CT DNA is non-intercalative. Next, the circular dichroism (CD) spectrum of QCY-DBT complexed with CT DNA was measured to confirm the binding mode. CD spectra of CT DNA alone displayed a positive and a negative signal at 280 and 245 nm (Fig. S10b in Supporting information), respectively. These characteristic CD signals confirm a typical B-form DNA duplex structure. With the increasing concentrations of QCY-DBT (0–0.54 mmol/L) to a fixed concentration of CT DNA (0.5 mg/mL), the CD spectra displayed strong induced positive CD signals at 602 nm and a negative signal at 493 nm in the absorption regions of QCY-DBT. Thus, the characteristic induced CD signal in the QCY-DBT absorption region revealed that the probe bound to the minor groove of CT DNA. A molecular docking simulation was also performed to reveal the mechanism of action between the probe and nucleic acids. The X-ray crystal structures of double-stranded DNA (dsDNA) (3rn5), dsRNA (3vyy), and single-stranded RNA (ssRNA) (6 gbm) collected from the PDB database were chosen to be docked with QCY-DBT using the Local Search Parameters module in AutoDock 4.2. QCY-DBT bound to the groove of dsDNA and dsRNA (Fig. S10c in Supporting information). The binding energy of QCY-DBT with dsDNA (6.27 kcal/mol) was much higher than with dsRNA (2.79 kcal/mol) or ssRNA (2.71 kcal/mol) (Table S2 in Supporting information). Therefore, QCY-DBT had a better binding ability to DNA groove than RNA, consistent with the data from the nucleic acid response experiments in solution (Fig. 1c).

The selective fluorescence enhancement of QCY-DBT in the presence of CT DNA further encouraged us to study its cellular uptake and nucleic acid staining in living cells. To check its permeability, we conducted cellular uptake studies in five kinds of cells, including cancer (MCF-7, HepG2, 4T1) and normal cell lines (3T3, GES-1). QCY-DBT possessed good cell permeability and only localized in the cytosol, based on the cellular imaging data (Fig. S11 in Supporting information). To further reveal the subcellular localization of QCY-DBT, colocalization experiments were first conducted in MCF-7 cells, and the red signal of QCY-DBT nicely coincided with the green fluorescence of the mitochondrial tracking dye (Person's coefficient 0.94) (Fig. S12 in Supporting information). In addition, similar results were found in other cell lines (HepG2, 4T1, 3T3, and GES-1) (Fig. S13 in Supporting information), confirming that QCY-DBT is an excellent mitochondria-targeted probe in living cells. To further determine whether QCY-DBT stained mtDNA, fixed MCF-7 cells were treated with DNase or RNase, which catalyze DNA or RNA hydrolysis, respectively (Fig. S14 in Supporting information). When the cells were treated with RNase, the fluorescence signal of QCY-DBT was the same as in the control. However, cells treated with DNase exhibited almost no fluorescence signal of QCY-DBT and Hoechst 33342. Meanwhile, the cells were treated with DNase (100.0 U/mL) at different time points (0, 15, 30, and 90 min) in the DNA experiment (Fig. S15 in Supporting information). As the incubation time of DNase increased, the fluorescence intensity of QCY-DBT decreased, demonstrating that QCY-DBT could detect mtDNA content in living cells. These results confirmed that QCY-DBT was suitable for the specific and highly sensitive visual imaging of mtDNA in living cells.

Cell apoptosis leads to the depletion of mtDNA [45]. Since the reduction of the transmembrane potential of the mitochondria is an inevitable event during cell apoptosis, the location of QCY-DBT should not be related to mitochondrial membrane potentials during cell apoptosis. To confirm this hypothesis, MCF-7 cells were incubated with QCY-DBT and Mito Tracker Green^{FM} (a commercial mitochondrial probe independent of mitochondrial membrane potential) for 30 min each. Then, MCF-7 cells were treated with carbonyl cyanide 3-chlorophenylhydrazone (CCCP), mitochondrial membrane polarization inducer, 50.0 μmol/L) to reduce the mitochondrial membrane potential (Fig. S16 in Supporting information). We found that Pearson's coefficient of QCY-DBT with Mito Tracker Green^{FM} was almost unchanged. Next, MCF-7 cells were co-incubated with JC-1 (mitochondrial membrane potential probe)

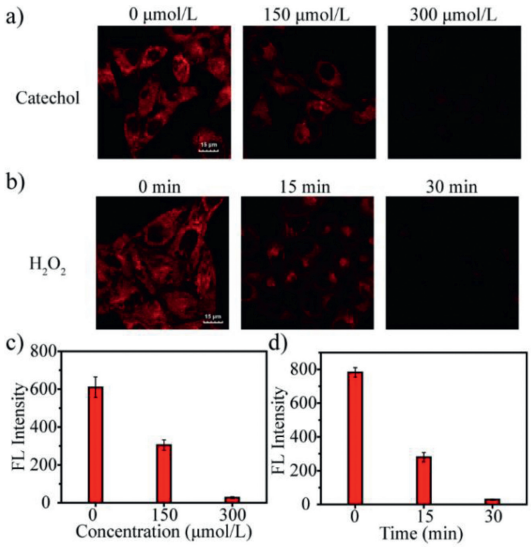

Fig. 2. (a) Fluorescence microscopy images of MCF-7 cells during cell apoptosis. The apoptosis models were established by catechol at different concentrations (0, 150, and 300 μmol/L). Scale bar: 15 μm. (b) Fluorescence microscope images of MCF-7 cells during cell apoptosis. The cell apoptosis models were established using H_2O_2 (0.4 mmol/L) at different incubation times (0, 15, and 30 min). Scale bar: 15 μm. (c) Intracellular average fluorescence intensity of QCY-DBT as observed in (a). (d) Intracellular average fluorescence intensity of QCY-DBT as observed in (b). For the red channel, the emission was collected at 650–700 nm ($\lambda_{ex} = 561$ nm).

and QCY-DBT for 30 min, and then the cells were treated with CCCP. As indicated in Fig. S17 (Supporting information), the fluorescence intensity of JC-1 increased significantly with the increase of CCCP co-incubation time, while the fluorescence intensity of the QCY-DBT remained unchanged. Similar results were also observed in HepG2, 4T1, 3T3, and GES-1 cells (Fig. S17), demonstrating that the monitoring of mtDNA by QCY-DBT during cell apoptosis was unaffected by changes in mitochondrial membrane potentials.

These results encouraged us to verify further whether QCY-DBT can discriminate healthy cells from apoptotic ones. Apoptosis in MCF-7 cells was induced by different concentrations of catechol (0, 150, 300 μmol/L) (Figs. 2a and c) or different treatment times (0, 15, 30 min) with hydrogen peroxide (H_2O_2, 0.4 mmol/L) (Figs. 2b and d). The fluorescence intensity of QCY-DBT decreased significantly with an increase in the degree of apoptosis (Fig. 2). Similar results were found in other cell lines (HepG2, 4T1, 3T3, and GES-1) (Figs. S18 and S19 in Supporting information). The extent of mtDNA damage increases continuously in living cells with the degree of cell apoptosis. Therefore, the content in mtDNA that could bind to QCY-DBT decreases as the degree of apoptosis progresses, resulting in a continuous decrease in the fluorescence intensity. All the above results have confirmed that QCY-DBT could assess apoptotic cells in real time by monitoring changes in intracellular mtDNA.

Due to the ultrasensitivity for DNA, we anticipated that QCY-DBT was suitable for detecting WBCs [41]. Thus, QCY-DBT was configured as a kit for WBC analysis. The kit contains a fluorescent probe storage solution (QCY-DBT, 10 mmol/L in ethanediol), a red blood cell lysis buffer (LB, selectively lysed RBCs and left the leukocytes), and a spherical reagent buffer (SRB, improved the permeability of cell membranes). When WBCs and RBCs were treated with QCY-DBT, QCY-DBT only selectively stained WBCs and did not respond to RBCs (Fig. S21 in Supporting information). Then, the kit was applied to analyze human peripheral blood cells in flow cytometry (Fig. S22 in Supporting information). Blood cells could not be classified in the control group (no probe) (Fig. S22a). After incubating QCY-DBT (0.88 μmol/L) with blood cells (20 μL) in LB (1 mL) for only 10 s, five parts were observed: monocytes, lymphocytes, neutrophils, eosinophils, and blood shadow (Figs. S22c and f). The semblable results are presented in the ZX-DIFF (commercial probe for WBCs, Fig. S20 in Supporting information) group (Figs. S22b and e). The count of four kinds of WBCs in the QCY-DBT group was almost unchanged compared to the ZX-DIFF group (Fig. S22d). Optimal imprecision was observed for all the parameters tested in Table S3 (Supporting information), and most of the coefficients of variations (CV) of QCY-DBT were below 10%. These results revealed the identical WBC classification ability of QCY-DBT with ZX-DIFF. To analyze RBCs, blood cells were first treated with 1 mL SRB and then stained with QCY-DBT for only 20 s. Compared with commercial probe ZX-RET (Fig. S20) for the analysis of RETs, immature erythrocytes could not be detected in the direction of fluorescence by QCY-DBT (Figs. S22g–i). These results indicate that QCY-DBT could separate and classify WBCs from human peripheral blood cells and have no response to RBCs.

The commercial probe (ZX-RET) for immature erythrocytes is excited at 630 nm and has a small stokes shift. When excited at 630 nm, the emission wavelength of QCY-DBT was longer than that of ZX-RET (Fig. S23 in Supporting information). In addition, QCY-DBT possessed an excellent analysis ability of WBCs and no response to immature erythrocytes. Therefore, it is possible to combine QCY-DBT with ZX-RET to simultaneously detect four kinds of WBCs and immature erythrocytes (reticulocytes, RETs). Encouraged by this proposition, a novel hematology analysis kit for WBCs and RBCs was configured, containing fluorescence probe stock solution 1 (QCY-DBT, 10 mmol/L in ethanediol), fluorescence probe stock solution 2 (ZX-RET, 20 μmol/L in ethanediol), LB, and SRB. The kit was studied in flow cytometry to analyze peripheral blood cells and predict the possibility of detecting multiple blood cells. As indicated in Fig. 3a, blood cells could not be classified in the control group (no probe), and WBCs could not be classified by the ZX-RET group (Fig. 3b). Four kinds of WBCs were observed in the QCY-DBT + ZX-RET group, consistent with the QCY-DBT group (Figs. 3c–e). In addition, four kinds of WBCs were counted in Fig. 3j, and the results agreed with the commercial probe (CV < 10%) (Table S4 in Supporting information). As for the analysis of RETs, the QCY-DBT + ZX-RET group presented a similar result as the ZX-RET group, indicating the excellent immature erythrocyte detection ability in flow cytometry (Figs. 3f–i and Table S4). Furthermore, as indicated in Fig. 3i, PLTs were also detected in the QCY-DBT + ZX-RET group. Together, the results demonstrated the ability of the novel kit to detect and analyze multiple human peripheral blood cell.

The fact that the pH response signal of QCY-DBT was amplified by DNA in solution further motivated us to distinguish cancer cells from normal cells by looking into the pH changes. When entering the living cells, the pH response signal of QCY-DBT would be amplified by mtDNA. To simulate the acidic microenvironment of the tumor, cancer cells (MCF-7, 4T1, and HepG2) were pretreated with an acidic medium (pH 6.0). After incubation with QCY-DBT for 30 min, a higher fluorescence intensity (~2.02-fold) was observed in cancer cells than in normal cells (Fig. 4). These imaging phenomena are consistent with the results in the solution, further indicating that QCY-DBT could be applied as a pH-sensitive fluorescent probe selective for differentiating cancer cells from normal cells.

In summary, by incorporating *N*-benzyl-2-methylbenzothiazolium bromide salt into 4-hydroxyisophthalaldehyde, we created an mtDNA-triggered and pH response signal-amplified NIR fluorescent probe, named QCY-DBT, which displays a large stokes shift and outstanding selectivity and sensitivity for mtDNA. QCY-DBT was successfully applied for *in-situ* monitoring of apoptotic cells and detecting four kinds of WBCs and immature erythrocytes in human peripheral blood cells. In addition, mtDNA could amplify

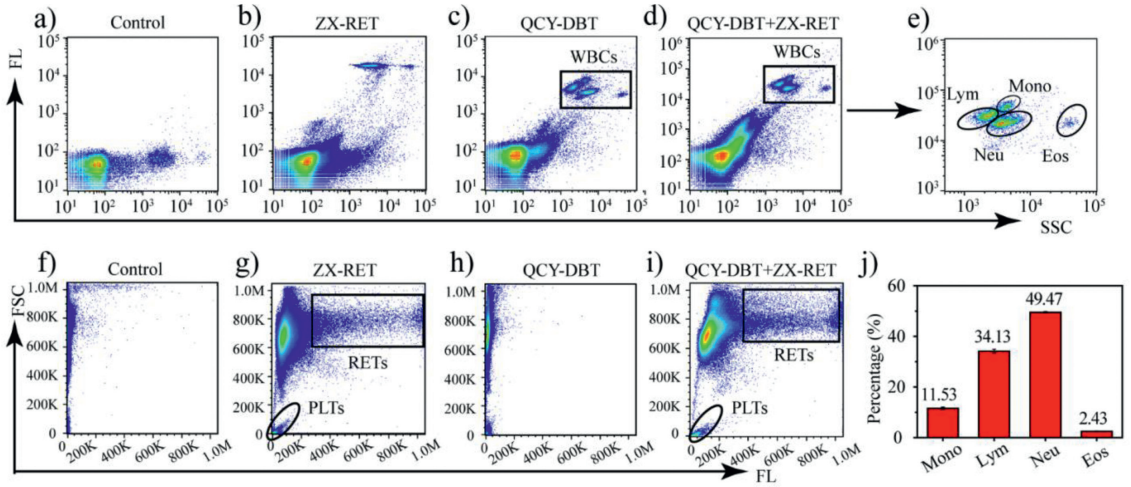

Fig. 3. Analysis of peripheral blood cells in flow cytometry. (a) Peripheral blood cells (20 μL) were treated only with LB (1 mL). (b) Peripheral blood cells (20 μL) were treated with LB (1 mL) and ZX-RET (0.88 μmol/L) for 10 s (the excitation wavelength was set at 637 nm, and fluorescence signals were read at 670 ± 14 nm). (c) Peripheral blood cells (20 μL) were treated with LB (1 mL) and QCY-DBT (0.88 μmol/L) for 10 s (the excitation wavelength was set at 637 nm, and fluorescence signals were read at 670 ± 14 nm). (d) Peripheral blood cells (20 μL) were treated with LB (1 mL), and QCY-DBT (0.88 μmol/L) and ZX-RET (0.88 μmol/L) were added for 10 s (the excitation wavelength was set at 637 nm, and fluorescence signals were read at 670 ± 14 nm). (e) Details of WBCs in (d). (f) Peripheral blood cells (4 μL) were treated only with SRB (1 mL). (g) Peripheral blood cells (4 μL) were treated with SRB (1 mL) and ZX-RET (0.39 μmol/L) for 20 s. (h) Peripheral blood cells (4 μL) were treated with SRB (1 mL) and QCY-DBT (0.39 μmol/L) for 20 s. (i) Peripheral blood cells (4 μL) were treated with SRB (1 mL), and QCY-DBT (0.39 μmol/L) and ZX-RET (0.39 μmol/L) were added for 20 s. (j) The count of the four kinds of WBCs in (e).

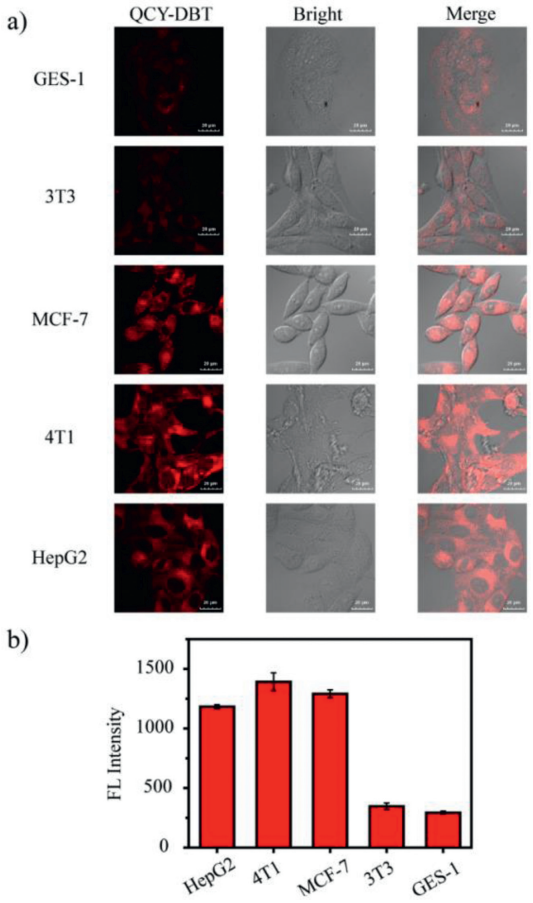

Fig. 4. (a) Fluorescence microscopy images of QCY-DBT (4 μmol/L) in normal cells (GES-1 and 3T3) and cancer cells (MCF-7, 4T1, and HepG2). Cancer cells were pretreated with an acid medium (pH 6.0). (b) Intracellular average fluorescence intensity of QCY-DBT in (a). For the red channel, the emission was collected at 650–700 nm (λ_{ex} = 405 nm). Scale bar: 20 μm.

the fluorescence signal of QCY-DBT to pH (6.0–7.4) and make it distinguish cancer cells successfully. All these results suggested QCY-DBT could potentially serve as an effective tool for tracking the physiological state of cells in complex biosystems and further for diagnosing related diseases.

Declaration of competing interest

The authors declare that they have no known competing financial interests or personal relationships that could have appeared to influence the work reported in this paper.

Acknowledgments

This work was financially supported by the National Key Research and Development Plan (No. 2018AAA0100301), National Science Foundation of China (No. 21925802), Research Funds for the Central Universities (No. DUT22LAB601) and the Basic Research Project of Free Exploration (No. 2021Szvup019).

Supplementary materials

Supplementary material associated with this article can be found, in the online version, at doi:10.1016/j.cclet.2023.108577.

References

[1] B.H. Foy, T.M. Sundt, J.C.T. Carlson, et al., Nat. Commun. 13 (2022) 4705.
[2] B.H. Shaz, Blood 133 (2019) 2627–2628.
[3] I.A. Elcheva, V.S. Spiegelman, Leukemia 35 (2021) 360–376.
[4] O. Okocha, H. Dand, M.J. Avram, B. Sweitzer, Anesthesiology 133 (2020) 109–118.
[5] J. Huang, M. Gendy, M. Wronska, et al., Blood 136 (2020) 10–11.
[6] B. Kim, Y.J. Choi, H. Seo, et al., Small 12 (2016) 5159–5168.
[7] L. Zhao, P. Sumberaz, Chem. Res. Toxicol. 33 (2020) 2491–2502.
[8] N. Tahbaz, S. Subedi, M. Weinfeld, Nucleic Acid. Res. 40 (2012) 3484–3495.
[9] P. Sharma, H. Sampath, Cells 8 (2019) 100.
[10] C. Li, C. Zong, Y. Liu, et al., Chin. Chem. Lett. 35 (2024) 108323.
[11] A.S. Tan, J.W. Baty, L.F. Dong, et al., Cell Metab. 21 (2015) 81–94.
[12] M. Jiang, X. Xie, X. Zhu, et al., Sci. Adv. 7 (2021) 8631–8647.
[13] K. McArthur, L.W. Whitehead, J.M. Heddleston, et al., Science 359 (2018) 6047–6058.
[14] M. Higurashi, T. Maruyama, Y. Nogami, et al., Exp. Cell Res. 389 (2020) 111889.

[15] T.C. Kenny, M.L. Gomez, D. Germain, Cancer Res. 79 (2019) 6057–6066.
[16] Y. Dai, C. Xu, X. Sun, X. Chen, Chem. Soc. Rev. 46 (2017) 3830–3852.
[17] X. Luo, H. Yang, H. Wang, et al., Anal. Chem. 90 (2018) 5803–5809.
[18] J. Qiu, C. Zhong, M. Liu, et al., Sens. Actuat. B: Chem. 371 (2022) 132606.
[19] X. Wang, L. Wang, T. Jin, et al., Sens. Actuat. B: Chem. 375 (2023) 132935.
[20] S. Fan, J. Xu, Y. Osakada, et al., Chem 8 (2022) 3109–3119.
[21] B. Li, Y. Wang, M.H. Chan, et al., Angew. Chem. Int. Ed. 61 (2022) 202210703.
[22] X. Liu, Y.T. Chang, Chem. Soc. Rev. 51 (2022) 1573–1591.
[23] Y. Zhao, H.S. Kim, X. Zou, et al., J. Am. Chem. Soc. 144 (2022) 20854–20865.
[24] T.B. Ren, Z.Y. Wang, Z. Xiang, et al., Angew. Chem. Int. Ed. 60 (2021) 800–805.
[25] J. Yan, X. Liang, Q. Zhang, et al., Chin. Chem. Lett. 35 (2024) 108408.
[26] K. Li, S. Wu, G. Dong, et al., Chin. Chem. Lett. 34 (2023) 108231.
[27] Q. Zhou, S. Wang, X. Ran, et al., Chin. Chem. Lett. 34 (2023) 107922.
[28] D. Ma, T. Liu, Q. Yao, X. Peng, Sci. China Chem. 61 (2018) 468–475.
[29] K. Uno, N. Sugimoto, Y. Sato, Nat. Commun. 12 (2021) 2650.
[30] W. Long, B.X. Zheng, X.H. Huang, et al., J. Med. Chem. 64 (2021) 2125–2138.
[31] C.E. Elgar, N.A. Yusoh, P.R. Tiley, et al., J. Am. Chem. Soc. 145 (2023) 1236–1246.
[32] F. Gao, L. Li, J. Fan, et al., Anal. Chem. 91 (2019) 3336–3341.
[33] K. Wang, S. Yan, T. Han, et al., J. Am. Chem. Soc. 144 (2022) 11788–11801.
[34] H. Yang, J. Chen, Y. Liang, et al., ACS Appl. Mater. Interfaces 13 (2021) 45291–45299.
[35] Y. Zhang, Y. Takahashi, S.P. Hong, et al., Nat. Commun. 10 (2019) 5610.
[36] W. Su, D. Yang, Y. Wang, et al., Nano Res. 15 (2022) 5193–5204.
[37] C. Villa, M. Campione, B. Santiago-Gonzalez, et al., Adv. Funct. Mater. 28 (2018) 1707582.
[38] J. Wang, F. Huo, Y. Zhang, C. Yin, Chin. Chem. Lett. 34 (2023) 107818.
[39] Y. Liu, L. Teng, C. Xu, et al., Chem. Sci. 10 (2019) 10931–10936.
[40] M. Chen, C. Wang, Z. Ding, et al., ACS Cent. Sci. 8 (2022) 837–844.
[41] N. Jiang, J. Fan, F. Xu, et al., Angew. Chem. Int. Ed. 54 (2015) 2510–2514.
[42] R. Yang, X. He, G. Niu, et al., ACS Sens. 6 (2021) 1552–1559.
[43] N. Karton-Lifshin, E. Segal, L. Omer, et al., J. Am. Chem. Soc. 133 (2011) 10960–10965.
[44] K.M. Ririe, R.P. Rasmussen, C.T. Wittwer, Anal. Biochem. 245 (1997) 154–160.
[45] C.S. Burke, A. Byrne, T.E. Keyes, Angew. Chem. Int. Ed. 57 (2018) 12420–12424.